A00-16787

AIAA 00–0960

Large-Eddy Simulations of Combustion in Gas Turbine Combustors

S. Menon C. Stone V. Sankaran
School of Aerospace Engineering
Georgia Institute of Technology
Atlanta, Georgia 30332
and
B. Sekar
Wright Patterson AFB
Dayton, Ohio 45433

38th AIAA Aerospace Sciences Meeting and Exhibit
10 - 13 January, 2000 / Reno, NV

Large-Eddy Simulations of Combustion in Gas Turbine Combustors

S. Menon* C. Stone† V. Sankaran‡
School of Aerospace Engineering
Georgia Institute of Technology
Atlanta, Georgia 30332
and
B. Sekar§
Wright Patterson AFB
Dayton, Ohio 45433

A new parallel two-phase compressible 3-D flow solver has been recently developed to study high Reynolds number reacting flows in full-scale gas turbine combustors. The past studies established the ability of this solver to carry out accurate large-eddy simulations (LES) using relatively coarse grid resolution. Premixed combustion in the flamelet regime and non-reacting mixing due to spray vaporization were studied using this code. The present study continues the development of the simulation methodology and investigates issues related to the integration of detailed finite-rate kinetics into the LES solver. The use of In-situ Adaptive Tabulation (ISAT) to efficiently calculate multi-species finite-rate kinetics is demonstrated Application of global kinetics to study fuel-air mixing and combustion in a Trapped Vortex Combustor (TVC) is also discussed. These studies, along with the earlier development have established a LES methodology that can used to simulate complex reacting flows in gas turbine engines.

1 Introduction

Desirable features for the next generation gas turbine engines are combustion efficiency, reduced emissions and stable combustion in the lean limit. To reach these goals, current research is focusing on improving the liquid fuel atomization process and to increase fuel-air mixing downstream of the fuel injector. However, the structure of complex three-dimensional, swirling fuel-air mixing layers is very difficult to resolve using current experimental and numerical methods. Since fuel atomization and fuel-air mixing are both highly unsteady, conventional steady state methods cannot be used to elucidate the finer details. Here, an approach using large-eddy simulation (LES) is being developed for high Reynolds number (Re) flows.

In LES modeling of the momentum transport scales larger than the grid size are computed using a time- and space-accurate scheme, while the effect of the unresolved smaller scales (assumed to be mostly isotropic) on the resolved motion is modeled using an eddy viscosity based subgrid model. This approach is acceptable for momentum transport since all the energy containing scales are resolved and all the unresolved scales (that primarily provide for dissipation of the energy transferred from the large scales) can be modeled by using an eddy dissipation subgrid model. However, these arguments cannot be extended to reacting flows since, for combustion to occur, fuel and oxidizer species must first mix at the molecular level. Since, this process is dominated by the mixing process in the small-scales, ad hoc eddy diffusivity concepts cannot be used except under very specialized conditions. To deal with these distinctly different modeling requirements, a new subgrid mixing and combustion model has been developed that allows for proper resolution of the small-scale scalar mixing and combustion effects within the framework of a conventional LES approach.

The earlier studies[1-3] have established the ability of the LES model in premixed combustion and in fuel-air mixing. To reduce the computational cost, the past calculations employed flamelet models (for premixed combustion) or simulated fuel-air mixing without detailed chemical kinetics. However, for realistic simulations for the reacting flow, detailed finite-rate kinetics must be used, especially if pollutant formation is to be studied. As is well known, the computational effort involved when using detailed kinetics is so large as to make LES of even a simple configuration computationally infeasible. Typically, global kinetics are employed to reduce the computational cost. However, such kinetics are not able to deal with ignition and extinction processes and are also unable to accurately predict pollutant (NOx, CO and UHC) formation.

Recent development of skeletal mechanisms has af-

*Professor, AIAA Senior Member
†Graduate Research Assistant, AIAA Student Member
‡Graduate Research Assistant, AIAA Student Member
§AIAA Member

forded an opportunity to address these issues. Skeletal mechanisms are derived from the full mechanisms using sensitivity analysis and have been shown to be reasonably accurate over a wide range of equivalence ratio. Although typical skeletal mechanism is much smaller than a full mechanism (e.g., 20 species instead of 100+ species in the full mechanism), the computational cost is still exorbitant for LES application. Here, we demonstrate that a skeletal mechanism when combined with the ISAT approach is capable of achieving an order of magnitude (or more) reduction in computational cost without sacrificing accuracy.

This paper summarizes the effort in the last six months under the DoD High Performance Computing (HPC) Grand Challenge projects. Progress under these projects were recently reported[4,5] and therefore, are not repeated here. This paper addresses only the effort subsequent to these earlier reports.

2 Simulation Model

The compressible LES equations are obtained by Favre-filtering Navier-Stokes equations using a top-hat filter (appropriate for finite-volume schemes). The filtering process results in terms in the resolved LES equations that require modeling. The final LES equations are avoided here for brevity since they are described elsewhere.[6] In general, the subgrid terms representing the subgrid stress tensor, the subgrid heat flux, the subgrid viscous work, the subgrid species mass flux, and the subgrid enthalpy flux all require modeling.

The subgrid stresses in the LES momentum equations are modeled using an eddy viscosity, which in turn, is modeled in terms of the LES filter width Δ and the subgrid kinetic energy K^{sgs}.[7] A transport model equation for the subgrid kinetic energy is solved along with the other LES equations.[1,2,6,8] The effects of subgrid turbulence on flame structure (and propagation) in premixed combustion can be quantified in terms of the subgrid kinetic energy[1,9] and thus, it is advantageous to use this type of LES model for reacting flows. Another distinct advantage of this approach is that this model does not assume equilibrium between subgrid kinetic energy production and dissipation (implicit in algebraic models) and thus, helps to attribute a relaxation time associated with the non-equilibrium in the subgrid scales.

To handle the distinctly different physics of scalar mixing and chemical reactions a new subgrid model has been developed. Details of this model have been reported elsewhere[3,10-12] and therefore, only summarized here.

3 Finite-rate kinetics modeling

The structure of turbulent premixed flame has many facets in practical combustors due to widely varying turbulence-chemistry interactions that can occur. Premixed combustion in the flamelet, the corrugated flamelet and the distributed reaction (recently called the thin-reaction zones) regimes can coexist within the same device. Models used within large-eddy simulation (LES) methodology to simulate practical systems must therefore, be able to predict these space- and time-varying flame structure and propagation characteristics without requiring *ad-hoc* changes.

Simulations of realistic combustion systems using large-eddy simulations (LES) have also used flamelet models with reasonable success.[1-3,10,11,13] However, when detailed information of the chemical species distribution is required flame-turbulence interactions at all the relevant scales must be resolved. In order to do this, a model is needed that can be applied in the entire parameter space without requiring any *ad hoc* adjustments. In this study, the linear eddy mixing (LEM) model of Kerstein,[14] which was previously demonstrated for LES in the flamelet regime[3,10,23,24] is used to investigate the nature of flames over a wide range of operational parameters. The goal of this study is to demonstrate that LEM is capable of capturing the physics of these flames without any ad hoc fixes and therefore, is a viable LES subgrid combustion model.

The structure and propagation characteristics of a turbulent premixed flame depends in most part on the relative magnitude of the chemical and turbulent time and length scales. The ratio of the turbulence intensity u' to the laminar flame speed S_L and the ratio of the characteristic turbulent scales, e.g., the Kolmogorov scale η or the integral length scale L to the flame thickness δ_f have often been used to characterize the nature of premixed flame-turbulence interactions. Combustion diagrams such as the one shown in Figure 1 have been used to characterize the structure of the premixed flame.[15,16] Two regimes are of particular interest here. The flamelet regime is characterized by $\delta_f << \eta$ and thus, turbulence can only wrinkle the flame without affecting its structure. On the other hand, in the distributed reaction regime $\eta < \delta_f$ and turbulent eddies can penetrate into the flame thereby, modifying the flame structure.

Recent studies[17-19] have suggested that even in the distributed reaction regime the reaction zone is very thin and of the order of the laminar flame thickness. This result is derived from the observations that for large $Ka = (\delta_f/\eta)^2$ and Reynolds number $Re = u'L/\nu$ turbulent eddies can enter the preheat zone and thus, increase turbulent transport of heat and species away from it. This re-distribution can thicken the preheat zone. However, eddies do not penetrate into the reaction zone since they are dissipated by increased viscous dissipation near the flame. Using these results, the distributed reaction regime has been re-classified as the extended flamelet[17] or the thin-reaction-zones[20] regime. The key implication is that modified versions of flamelet models can be used in the thin-reaction-

zones regime, as recently described by Peters.[20]

We simulated the methane-air flames B1, F1, F2 and F3 that were recently studied.[18,19,21] The typical location of these flames are given in Figure 1. As shown, B1 is in the corrugated flamelet regime while the flames F3-F1 cover the entire regime in the distributed regime. Only flames B1 and F1 are discussed here. More details of this study is reported in a recent paper.[22]

3.1 Model Formulation

The details of the LEM model have been given elsewhere[10,14,23,24] and therefore, are only briefly summarized here. LEM is a stochastic model which treats reaction-diffusion and turbulent convection separately but concurrently. Reaction-diffusion processes evolve on a one-dimensional (1D) domain in which all the characteristic length scales in the turbulent field (from L to η) are fully resolved (6 cells are used to resolve η). The orientation of the 1D domain is in the direction of the scalar gradient[14] and within this domain, the equations governing constant pressure, adiabatic laminar flame propagation are solved. The deterministic simulation of the reaction-diffusion processes can be viewed as a local direct numerical simulation. As a result, the reaction rate terms do not require any closure.

Turbulent stirring of the scalar field is implemented as distinctly independent process that interrupts the deterministic evolution of the reaction-diffusion processes on the 1D domain. Stirring is implemented as stochastic re-arrangement events called triplet maps, each of which represents the action of a turbulent eddy on the scalar fields. It has been shown[14] that this mapping can capture correctly the physical increase in scalar gradient (without affecting the mean scalar concentration) due to eddy motion. Three parameters are needed to implement these turbulent stirring events: the typical eddy size, the eddy location within the 1D domain and the stirring frequency (event rate). The method to obtain these parameters are given elsewhere.[14]

3.2 Numerical Implementation

Methane-air flames similar to those in the experiments are studied here. In order to obtain a realistic chemical state over a wide range of operating conditions, a 15-step, 19-reaction skeletal mechanism[25] is employed. This mechanism (which included NOx kinetics) has been shown to be quite accurate over a wide range of equivalence ratios. It is also capable of predicting extinction and re-ignition which is particularly relevant here since the F1 flame is considered close to the extinction limit.[19] Table 1 summarizes the chemical species and reactions in this skeletal mechanism.

The numerical method is the same as in the earlier study[24] and therefore, only briefly summarized. To simulate a stationary flame, a moving observation window is used that translates with the flame brush to maintain approximately the same relative position between flame center and observation window (even though the flame propagates freely into the reactants). All statistics are obtained relative to the flame center. The computational domain is chosen large enough to fully capture this flame brush (typically $6L$). Earlier studies[23,24] and the present study show that statistically, stationary flames can be simulated using this approach.

A fractional operator splitting method[24,26] is used to first evolve (via molecular diffusion and turbulent stirring) the scalar equations (without the reaction terms) for a small time step δt to obtain the thermochemical state after mixing. Then the reaction system is integrated over δt to get the final scalar state. The reaction point problem is very stiff due to a wide range of characteristic chemical time scales and hence, the computational cost for the time integration can be very high. Here, the ISAT approach[25] is used to efficiently handle the finite rate kinetics.[27]

In ISAT, only the accessed region of the composition space which is a subset of the whole realizable region (the set of all possible combinations of compositions for a given number of species) is tabulated. This tabulation is done as a part of the simulation and when the same composition re-occurs, the table is searched and the stored information is retrieved using fast binary tree search algorithm. Since only the accessible region is stored, the overall time required to build, retrieve and store information reduces significantly. Further details of the ISAT algorithm is given elsewhere[27] and therefore, avoided here for brevity.

To further reduce computational cost, the present model was parallelized with message passing (needed for the solution of the reaction-diffusion equations) handled by MPI directives. For the chemistry point problem no communication is needed. Each processor builds a table for the composition that occurs inside its domain during the computation. This localizes the ISAT table to each processor and reduces the overall load (including search and retrieve time) for each processor (as opposed to building a single table for all the composition that occurs over the whole of the domain). All simulations were done on a 32 processor CRAY-T3E system.

Computational efficiency of ISAT is significant as reported earlier.[27] The size of the table and cost depend upon the error tolerance (which determined the allowable error in each of the scalar for a given initial state). For higher accuracy, this parameter should be low, leading to an increase in the total simulation time and storage. For a value of $\epsilon_{tol} = 0.0008$ a speed-up of around 30 in the chemical update is achieved by using ISAT. This is consistent with the speedup reported earlier.[27] Table 2 summarizes the present results.

3.3 Flame structure

Typical instantaneous images of the flame structure in terms of the temperature and the destruction rate of methane, $\dot{\omega}_{CH_4}$ for flames B1 and F1 are shown in Fig. (2a) and (2b), respectively. For comparison, a typical experimental snapshot of the temperature and CH in the F1 flame is shown in Fig. (2c). We use $\dot{\omega}_{CH_4}$ to identify the location of the reaction zone (CH is not available in the skeletal mechanism) since it has been shown to correlate well location of the reaction zone.[28] The transition from the flamelet (Flame B1) to the structure seen in the thin-reaction-zones regime is clearly apparent in these figures. For Flame B1, the preheat zone upstream of the flame zone is inert with its temperature close to the free stream value. However, as Ka and Re increases, eddies penetrate into the preheat zone and increase the temperature ahead of the flame brush. For flame F1, the temperature in the preheat zone increases. However, the reaction zone still remains localized and thin in all cases with $\dot{\omega}_{CH_4}$ peaking at location of steep temperature gradients. There is very good qualitative agreement of the temperature profiles with the experimental data.[19] The reaction zone thickness is estimated to be 0.16 mm, 0.21 mm and 0.27 mm for F1, F2 and F3 flames, respectively. These values are very close to the laminar flame thickness of 0.175 mm.[18] Experimental data[19] for CH suggests a value in the range 0.2-0.5 mm for the F3 and F1 flames.

Although the reaction zone is thin and of the order of the laminar flame thickness, the preheat zone is much large. Using the definition[19] that the preheat zone is between temperature 600 K and 1300 K, the thickness of the preheat zone is estimated as 2.2 mm, 1.92 mm and 1.92 mm for the flames F1, F2 and F3, respectively. In the recent experiments[19] the preheat zone thickness was estimated in the range 2-3.5 mm for Flame F1. Presence of such thin reaction zones, with thick preheat zone in front, is characteristic of flames in thin-reaction-zone regime. Note that $\eta = 0.05$ mm, 0.06 mm and 0.1 mm for the F1, F2 and F3 flames, respectively.[18] Thus, the preheat zone thickness is much larger than η.

Mean and variance of the reaction progress variable, $c = (T - T_u)/(T_b - T_u)$ where T_u and T_b are respectively, the reactant and product temperature have also been computed. The transition from flamelet to thin-reaction-zones regime combustion is best presented by the probability density function (PDF) of c. Figure (3a) and (3b) presents the PDFs at six different locations for flames B1 and F1, respectively. As expected, in the flamelet regime (flame B1), the PDF exhibits two peaks corresponding to unburnt and burnt gases, respectively. In this regime probability of the reactive states corresponding to the transition between reactants and products is small.

For the F1 flame, the PDF is not bimodal since the interaction between flame and turbulence is not entirely kinematic but also depends on the length scales. Small eddies that enter the preheat zone broaden the flame increasing the probability of intermediate values of progress variable. There is excellent qualitative agreement with the progress variable PDF's reported in[29] for flames in similar regimes.

The mean temperature profiles for the two flames are shown in Fig. (4) as a function of X/L (note the L is much larger for B1). A direct comparison shows that as Ka increases the flame brush thickness increases which results in a broadened mean temperature profile. An increase in preheat zone thickness can be observed as we move from flamelet to distributed regime. The thickness of the preheat zone is of the order of the integral length for all the F-flames. This suggests that eddy as large as L are involved in the transport of heat and mass from the reaction zone into the preheat zone.

4 LES of Trapped-Vortex Combustor

The TVC is a combustor design under investigation for IHPTET applications. In this concept, the combustion occurs in a vortex trapped within a cavity and past results suggest that this can increase flame stability. Figure 5 shows schematically, the combustor simulated in the present study.

Various studies into the application of cavity–flow interaction have been conducted in the past. Earlier[30] it was noted that a cavity–locked vortex entrains very little main–flow air and would result in a low exchange of mass and heat between the cavity and the main flow. Since combustion requires a continuous supply of reactants, fuel and air must be directly injected in the cavity to sustain the burning processes. However, direct injection (mass addition) can disrupt the flow dynamics, possibly resulting in cavity instability. Previous attempts at numerical modeling of the TVC,[31,32] noted the possibility of mixing–limited reactions in the TVC. For this reason, fuel/air mixing and its effect on combustion in the TVC is investigated in this study.

The model formulation and the various closure models are summarized in a recent paper[33] and therefore, not repeated here. In the following, we briefly highlight some of the salient features observed in this study.

To investigate the fluid dynamic mixing properties of the TVC, two cases (I & II) were conducted under identical conditions except that the air flow velocity at the inlet was changed from 20 m/s (case I) to 40 m/s (case II). Non-reacting mixing was studied with fuel is injected into the cavity with an equivalence ratio far above stoichiometric ($\phi = 4.4$). Thus, entrainment and mixing with the ambient air is critical in order to achieve efficient combustion.

To increase mixing rates, higher turbulence levels are also desired. Regions of high mean and, perhaps more importantly, high RMS velocities will tend to

enhance mixing rates. Therefore, we investigated the effect of increasing in the primary air flow rate.

For visualization, the time averaged and instantaneous velocity vectors for cases I & II are shown in Figs. 6(a) & 6(b), respectively. The higher annular flow rate (Fig. 6(b)) enhances the trapped-vortex strength, allowing for increased annular/cavity flow interaction. In the time averaged results, it is seen that two vortices are present for case I. In addition to a vortex rotating in the direction of the annular flow, the second vortex rotates in the reverse direction. However, these vortices are not observed in case II. Rather, only a single, large vortex rotates with the flow. The instantaneous images on the other hand do show transient vortices in the shear layer and in the cavity indicating a process of unsteady entrainment of the primary air from the inlet. As discussed elsewhere[33] and noted below, this turbulent mixing appears to be beneficial for fuel-air mixing.

Two reacting-flow cases (IV & V) were also used to investigate the impact of fuel/air mixing rates under reacting conditions. The primary equivalence ratio of the cavity jets in both cases was again 4.4 and the injection temperature was a slightly elevated value of $500K$. As observed by Sturgess *et al.*,[34] the cavity flow entrains relatively little annulus air and will tend to be fuel–rich under reacting flow conditions. This was confirmed by looking at the the mean fuel and oxygen mass fractions[33] (not shown here). For the low speed case, near the injection ports, the RMS values are much higher due to fluctuations in velocity and species composition. Far from the injectors, however (near the fore-body wall), the oxygen is almost entirely consumed leaving a fuel–rich cavity region. The remaining fuel is finally consumed outside the cavity in either the dump shear layer or downstream of the after-body, depending on the inlet flow velocity. For the higher flow velocity, on the other hand, more fuel is consumed in the cavity. This indicates that the primary air stream is entrained more with increase in flow velocity and the increase turbulence enhances fine-scale mixing.

The rate at which the fuel is mixed can be viewed by examining the species mixture fraction, Z, as a function of inflow velocity. Shown in Figs. 7(a) and 7(b) are the instantaneous and time averaged stoichiometric mixture fraction surfaces, $Z = Z_{st}$, for both reacting flow cases (The stoichiometric surface, Z_{st}, has been highlighted by a single black line, where Z_{st} for methane air is approximately 0.055). As can be seen in Fig. 7(b) (U_o = 40 m/s), Z_{st} is almost entirely contained inside the cavity region for both the instantaneous and the time averaged results. For the lower inflow velocity, the surface extends far downstream of the cavity zone.

Also shown in Figs. 7(a) and 7(b) are the instantaneous and time-averaged temperature color contours for cases IV & V . Following the same trends as Z, the peak temperature regions are seen to shift from outside the cavity region for a lower annular velocity to inside the cavity in case V. In both mean and instantaneous views, the cavity temperature increases with increased flow velocity.

Comparisons with experimental data is possible for case V. The mean and RMS temperature profiles reported by Hsu *et al.*[30] (obtained with the *CARS* technique) are super-imposed in Fig. 8. The combustor conditions were nearly identical to those simulated in case V, U_o = 42 m/s, ϕ = 4.4, H/d = 0.59; however, propane instead of methane was used as the primary fuel. Despite this difference, the mean temperature trends should still be comparable. A maximum instantaneous temperature of 2025 K was obtained inside the cavity in case II which is slightly lower then the 2150 K reported by Hsu *et al.*[30]

For both inflow velocities, the mean temperature near the injection ports has not been greatly effected. However, away from the injectors, the higher inflow velocity resulted in higher cavity temperatures for both mean and instantaneous profiles. The peak temperature region for the case IV is not inside the cavity but downstream in the after-body wake resulting in longer thermal residence times. The longer residence times may increase thermal NO_x production. As would be expected with the higher inflow velocity, the downstream temperature is lower despite higher cavity temperatures. This mainly due to the higher volume flow rate and lower overall equivalence ratio. The combination of a higher fuel consumption rate and higher velocity results in a lower thermal residence time. This is beneficial to lower combustion pollutant formation.

5 LES of full-scale combustor flows

Earlier studies of premixed combustion in the GE LM6000 were carried out using a flame speed model that did not account for flame broadening effects.[1] Recent studies[2] have extended this study to allow for flame stretch effects. Figure 9 shows the schematic of this combustor. For premixed combustion, highly swirling lean premixed reactants (methane-air) enter the square combustor (the shape was primarily dictated by experimental measurement requirements) from a circular pipe at a preheated condition of 600 K. The test conditions are typical of actual full-scale operation: Re (based on inlet diameter) of 330000, Swirl Number of 0.56, Karlovitz Number of 42 and Damkohler Number of 8.

Figure (10a) shows the mean axial velocity variation along the centerline and Fig. (10b) shows the mean radial velocity variation at x/D_0 = 0.18. Note that, hereafter, all velocity components (both mean and turbulence intensity) and the coordinates are nondimensionalized, respectively, by the maximum mean axial velocity at the inlet (U_0) and the inlet jet di-

ameter (D_0). The dynamic Pocheau's model when combined with the broadened-flame model (PBD20) predicts the mean axial velocity variation most accurately in comparison with the experiment. Different values of β do not significantly affect this agreement and $\beta = 20$ shows the best agreement with the experimental data. The agreement with the radial velocity is also reasonable.

A stringent test of LES is the ability to predict the turbulent fluctuation levels. This ability is highly dependent on the accurate characterization of the inflow turbulence (not much is known about the inflow turbulence in the experiments). Figure (11a) and (11b) show respectively, the root-mean-square (RMS) profiles of the fluctuating axial (u_{rms}) and radial (w_{rms}) velocity components. generated in this region due to the unsteady motion of the flame. The agreement is reasonable considering the many uncertainties involved.

6 Conclusions

The results of our LES model development effort subsequent to the progress reported earlier[4,5] is summarized in this paper. The past studies established the ability of this solver to carry out accurate large-eddy simulations (LES) using relatively coarse grid resolution. Premixed combustion in the flamelet limit and non-reacting mixing due to spray vaporization were studied using this code in full-scale combustors. The present study has addressed in particular, the issues related to the integration of detailed finite-rate kinetics into the LES solver. The use of In-situ Adaptive Tabulation (ISAT) to efficiently calculate multi-species finite-rate kinetics is demonstrated in this study. It is also demonstrated that the LEM model can be used to simulate premixed combustion irregardless of the nature of the flame structure (i.e., flamelet or thin-reaction-zones) without requiring any ad hoc fixes. This study when combined with the earlier studies clearly suggest that subgrid combustion modeling for LES is a viable option even when finite-rate kinetics is to be simulated.

Acknowledgments

This work was supported by the Army Research Office under the Multidisciplinary University Research Initiative. Computational time was provided by DOD High Performance Computing Centers at NAVO, MS and SMDC, AL and WPAFB, OH under DOD Grand Challenge Projects.

References

[1] Kim, W.-W., Menon, S., and Mongia, H. C., "Large-Eddy Simulation of a Gas Turbine Combustor Flow," *Combustion Science and Technology*, Vol. 143, 1999, pp. 25–62.

[2] Kim, W.-W. and Menon, S., "Numerical Simulations of Turbulent Premixed Flames in the Thin-Reaction-Zones Regime," *Combustion Science and Technology (to appear)*, 1999.

[3] Chakravarthy, V. and Menon, S., "Large-Eddy simulations of turbulent premixed flames in the flamelet regime," Combustion Science and Technology (submitted).

[4] Menon, S., Kim, W.-W., Chakravarthy, V. K., Pannala, S., and Henry, W., "Parallel Simulations of Turbulent Reacting Sprays," *AIAA-99-3438*, 1999.

[5] Menon, S., Kim, W.-W., Stone, C., and Sekar, B., "Large-Eddy Simulation of Fuel-Air Mixing and Chemical Reactions in Swirling Flow Combustor," *AIAA-99-3440*, 1999.

[6] Kim, W.-W. and Menon, S., "A new incompressible solver for large-eddy simulations," *International Journal of Numerical Fluid Mechanics*, Vol. 31, 1999, pp. 983–1017.

[7] Schumann, U., "Subgrid Scale Model for Finite Difference Simulations of turbulent Flows in Plane Channels and Annuli," *Journal of Computational Physics*, Vol. 18, 1975, pp. 376–404.

[8] Kim, W.-W. and Menon, S., "A New Dynamic One-Equation Subgrid-Scale Model for Large-Eddy Simulations," *AIAA-95-0356*, 1995.

[9] Yakhot, V., "Propagation Velocity of Premixed Turbulent Flames," *Combustion Science and Technology*, Vol. 60, 1988, pp. 191–214.

[10] Menon, S., McMurtry, P., and Kerstein, A. R., "A Linear Eddy Mixing Model for Large Eddy Simulation of Turbulent Combustion," *LES of Complex Engineering and Geophysical Flows*, edited by B. Galperin and S. Orszag, Cambridge University Press, 1993.

[11] Smith, T. M. and Menon, S., "Subgrid Combustion Modeling for Premixed Turbulent Reacting Flows," *AIAA-98-0242*, 1998.

[12] Chakravarthy, V. and Menon, S., "Subgrid Modeling of Premixed Flames in the Flamelet Regime," Flow, Turbulance and Combustion (submitted).

[13] Menon, S. and Jou, W.-H., "Large-Eddy Simulations of Combustion Instability in an Axisymetric Ramjet Combustor," *Combustion Science and Technology*, Vol. 75, 1991, pp. 53–72.

[14] Kerstein, A. R., "Linear-Eddy Model of Turbulent Transport II," *Combustion and Flame*, Vol. 75, 1989, pp. 397–413.

[15] Borghi, R., "On the Structure and Morphology of Turbulent Premixed Flames," *Recent Advances in Aerospace Sciences*, edited by C. Casci and C. Bruno, Plenum Press, 1985, pp. 117–138.

[16] Peters, N., "Laminar Flamelet Concepts in Turbulent Combustion," *Twenty-First Symposium (International) on Combustion*, 1986, pp. 1231–1250.

[17] Poinsot, T., Veynante, D., and Candel, S., "Quenching processes and premixed turbulent combustion diagrams," *Journal of Fluid Mechanics*, Vol. 228, 1991, pp. 561–606.

[18] Chen.Y.C., Peters, N., Schneemann.G.A.i, Wruck.N.i, Renz.U., and ansour.M.S., "The Detailed Structure of Highly Stretched Turbulent Premixed Methane-Air Flames," *Combustion and Flame*, Vol. 107, 1996, pp. 223–244.

[19] Mansour, M., Peters, N., and Chen, Y., "Investigation of Scalar Mixing in the Thin Reaction Zones Regime using a simultaneous CH-LIF/Rayleigh Laser Technique," *Twenty-Seventh Symposium (International) on Combustion*, 1998, pp. 767–773.

[20] Peters, N., "The turbulent Burning Velocity for Large-scale and small scale turbulence," *Journal of Fluid mechanics*, Vol. 384, 1999, pp. 107–132.

[21] Bédat, B. and Cheng, R. K., "Experimental Study of Premixed Flames in Intense Isotropic Turbulence," *Combustion and Flame*, Vol. 100, 1995, pp. 486–494.

[22] Sankaran, V. and Menon, S., "Structure of Premixed Turbulent Flames in Flamelet and Thin-Reaction-Zone Regimes," *AIAA-00-0185*, 2000.

[23] Smith, T. and Menon, S., "One-dimensional simulations of freely propagating turbulent premixed flames," *Combustion Science and Technology*, Vol. 128, 1996, pp. 99–130.

[24] Smith, T. M. and Menon, S., "Model Simulations of Freely Propagating Turbulent Premixed Flames," *Twenty-Sixth Symposium (International) on Combustion*, 1996, pp. 299–306.

[25] Chen, J.-Y., Private Communication.

[26] Calhoon, W. H., Menon, S., and Goldin, G., "Comparison of Reduced and Full Chemical Mechanisms for Nonpremixed Turbulent H_2-Air Jet Flames," *Combustion Science and Technology*, Vol. 104, 1995, pp. 115–141.

[27] Pope, S., "Computationally Efficient implementation of combustion chemistry using in situ adaptive tabulation," *Combustion Theory Modelling*, Vol. 1, 1997, pp. 41–63.

[28] Najm, H. N., Paul, P. H., Mueller, C. J., and Wyckoff, P. S., "On the Adequacy of Certain Experimental Observables as Measurements of Flame Burning Rate," *Combustion and Flame*, Vol. 113, 1998, pp. 312–332.

[29] Duarte.D., Ferrao.P., and Heitor.M.V., "Turbulence Statistics and Scalar Transport in Highly Sheared Premixed flames," *Flow,Turbulence and Combustion*, Vol. 60, 1999, pp. 361–376.

[30] Hsu, K.-Y., Goss, L. P., and Roquemore, W. M., "Characteristics of a Trapped–Vortex Combustor," *Journal of Propulsion and Power*, Vol. 14, No. 1, 1998, pp. 1–12.

[31] Katta, V. and Roquemore, W., "Numerical studies on trapped–vortex combustor," *AIAA–96–2660*, 1996.

[32] Katta, V. R. and Roquemore, W. M., "Study of Trapped Vortex Combustor- Effect of Injection on Dynamics of Non-reacting and Reacting Flows in a Cavity," *AIAA 97-3256*, 1997.

[33] Stone, C. and Menon, S., "Simulation of Fuel-Air Mixing and Combustion in a Trapped Vortex Combustor," *AIAA-00-0478*, 2000.

[34] Sturgess, G. and Hsu, K.-Y., "Entrainment of mainstream flow in a trapped–vortex combustor," *AIAA-97-0261*, 1997.

Table 1 15 Step, 19 Species Mechanism

$H + 0.5O_2 = OH$
$H_2 + 0.5O_2 = H + OH$
$HO_2 = 0.5O_2 + OH$
$0.5O_2 + H_2O_2 = OH + HO_2$
$0.5O_2 + 0.5C_2H_2 = H + CO$
$CH_3 + CO + C_2H_4 = 0.5O_2 + CH_4 + 1.5C_2H_2$
$0.5O_2 + 2CH_3 = H_2 + CH_4 + CO$
$0.5O_2 + CH_3 = H + CH_2O$
$0.5O_2 + CH_4 = OH + CH_3$
$0.5O_2 + CO = CO_2$
$0.5O_2 + C_2H_6 = CH_4 + CH_2O$
$H + OH = H_2O$
$H + CH_4 + NO + HCN = 0.5O_2 + 2CH_3 + N_2$
$H + 0.5O_2 + CH_4 + HCN = 2CH_3 + NO$
$0.5O_2 + CH_4 + NH_3 + HCN = H_2O + 2CH_3 + N_2$

Table 2 ISAT Performance

	ϵ_{tol} = 5E-3	ϵ_{tol} = 8E-3	DI
Total CPU time	16.66 h	9.46 h	31.11 h
Chemistry time	0.0108 s	7.3e-3 s	0.2278 s
Speed up in Chemistry	21	31	-
Speed up in simulation	2	3	-
No. of Records	40500	16500	-

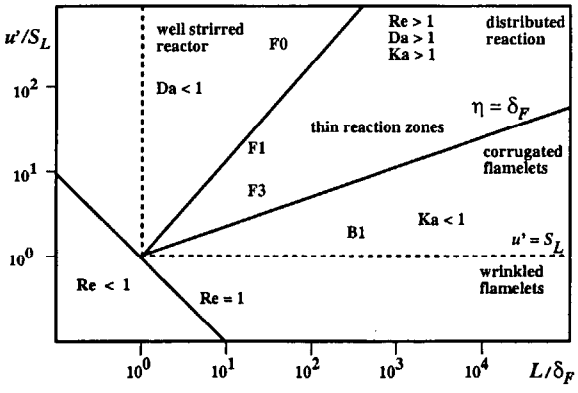

Fig. 1 Diagram of turbulent premixed combustion regimes. The location of the flames simulated in the present study are also shown.

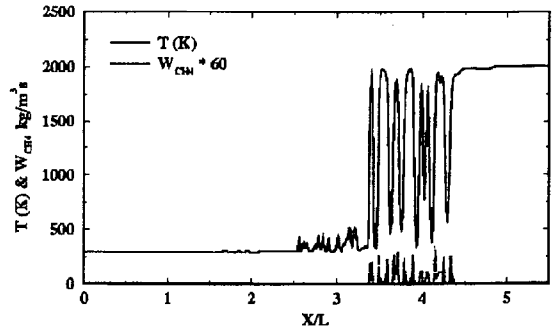

a) Flame B1

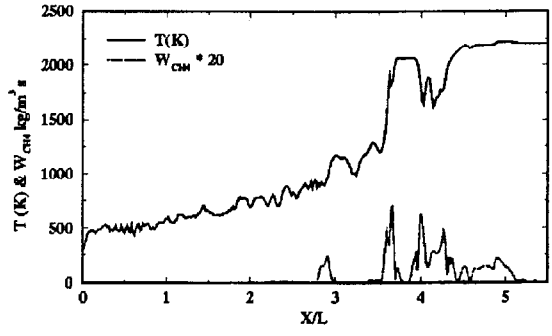

b) Flame F1

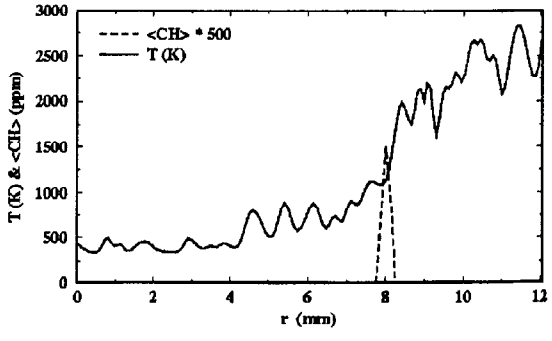

c) Flame F1 from Mansour *et al*[19]

Fig. 2 Instantaneous temperature and $\dot{\omega}_{CH_4}$ for the flames, B1, and F1 . Scale of $\dot{\omega}_{CH_4}$ is changed for ease of presentation.

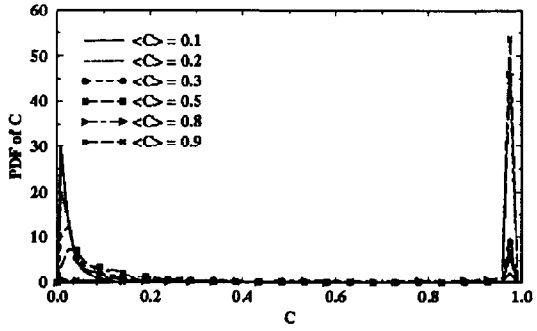

a) Flame B1

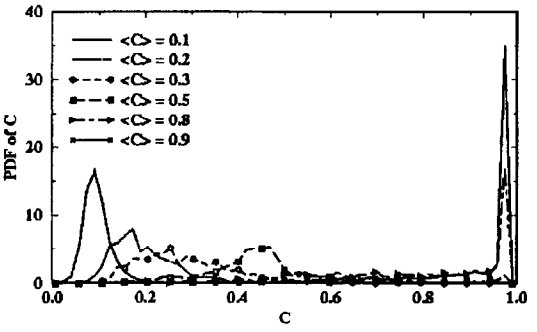

b) Flame F1

Fig. 3 PDF of the progress variable c at six different locations in the B1 and F1 flames. The transition from flamelet structure to the thin-reaction-zones flame structure is apparent in these PDFs.

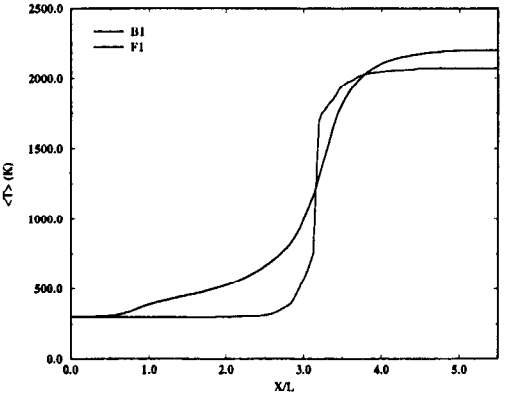

Fig. 4 Mean temperature across the flame brush.

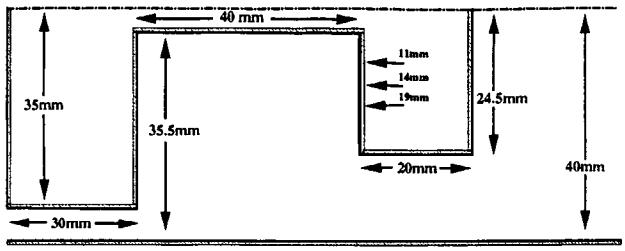

Fig. 5 Trapped–Vortex geometry used in this numerical study. Total length (x) = 285mm.

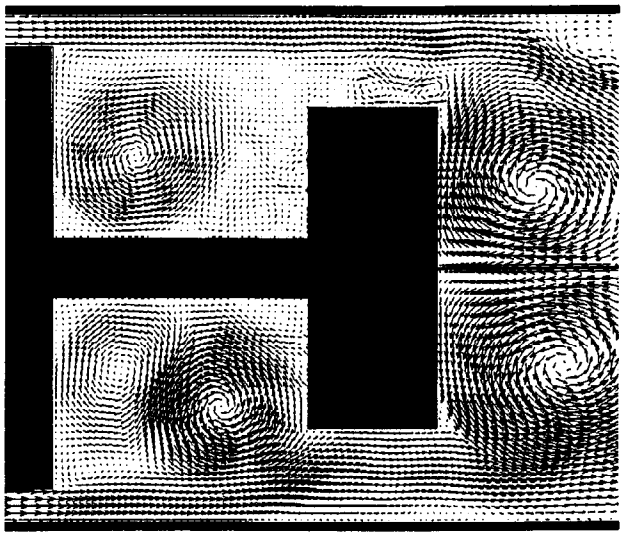

a) U_o = 20 m/s

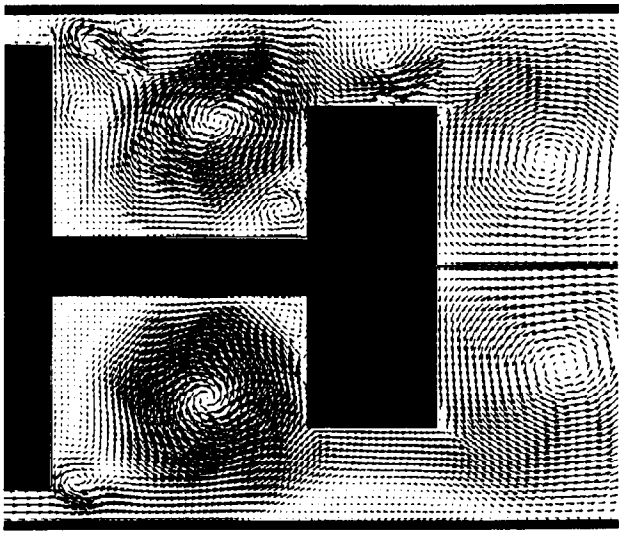

b) U_o = 40 m/s

Fig. 6 Non-Reacting velocity vectors for U_o = a) 20 m/s, b) 40 m/s (cases I & II). Upper halves are instantaneous, lower halves are time averaged.

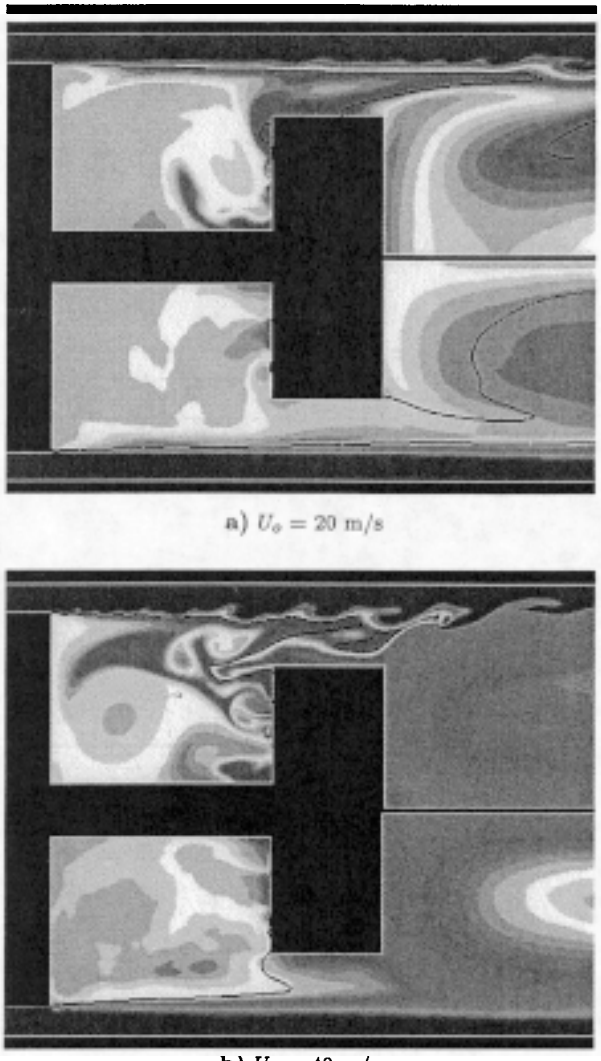

a) $U_o = 20$ m/s

b) $U_o = 40$ m/s

Fig. 7 Reacting flow temperature field and stoichiometric surface for U_o = a) 20 m/s, b) 40 m/s. Upper halves are instantaneous, lower halves are time averaged. Temperature color contour ranges are 300 K (blue) and 2000 K (red). Stoichiometric mixture fraction, $Z = Z_{st} \simeq 0.055$, shown with black line.

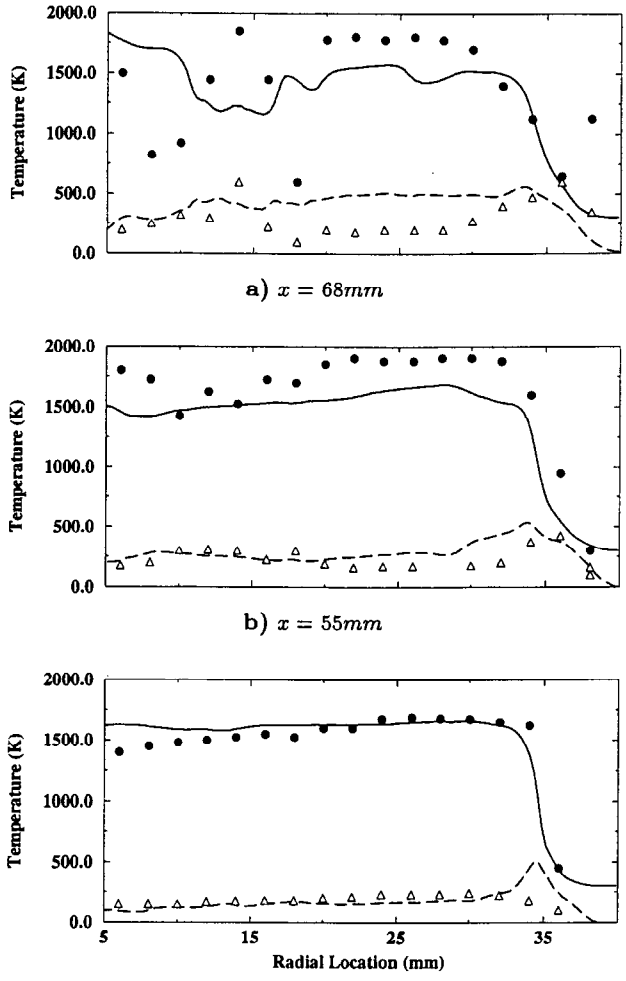

a) $x = 68mm$

b) $x = 55mm$

c) $x = 35mm$

Fig. 8 Mean and RMS temperature profiles at x = a) 68, b) 55, c) 35mm for U_o = 40 m/s (Case V). $< \widetilde{T} >$ (—), $\widetilde{T}^{RMS}$ (– –), T_{exp} (•), T_{exp}^{RMS} (△). Experimental results ($_{exp}$) from Hsu *et al.*[30]

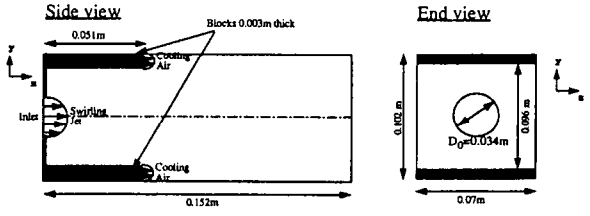

Fig. 9 Schematic of the LM-6000 being tested at General Electric

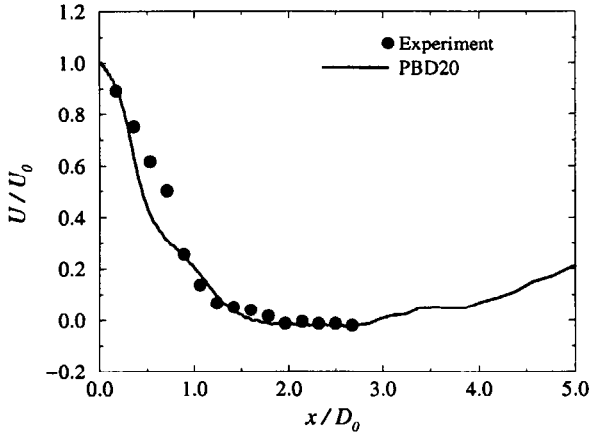

a) Mean axial velocity variation along the centerline

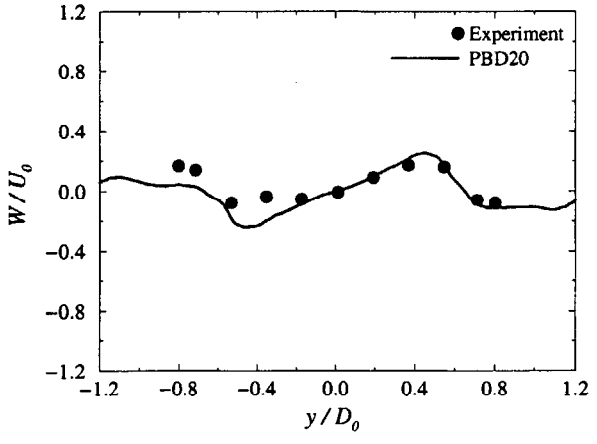

b) Mean radial velocity variation along y-axis at $x/D_0 = 0.18$

Fig. 10 Prediction of mean axial and radial velocity variation in the LM6000. Here, PBD20 denotes the test case that employed a local dynamic broadened flame speed model.

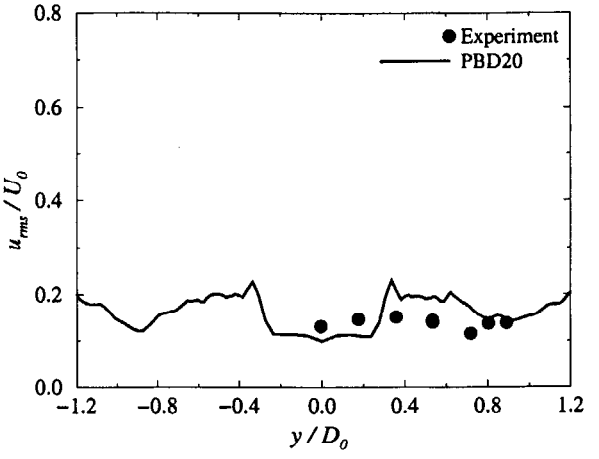

a) Axial velocity fluctuation intensity along y-axis at $x/D_0 = 0.18$

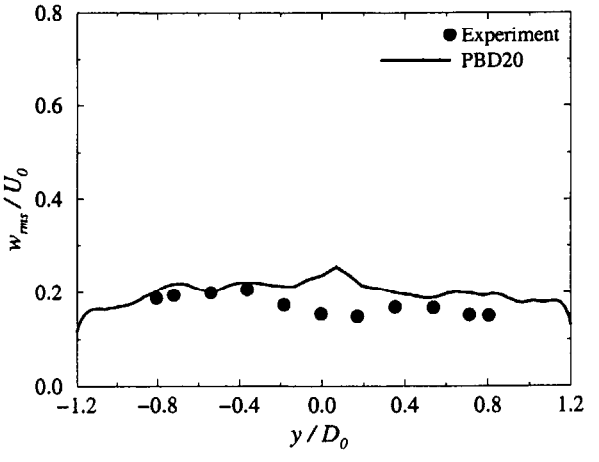

b) Radial velocity fluctuation intensity along y-axis at $x/D_0 = 0.72$

Fig. 11 Prediction of axial and radial velocity fluctuations in the LM6000